doi:10.1016/j.jmb.2007.01.015 J. Mol. Biol. (2007) 367, 692–701

JMB

Available online at www.sciencedirect.com

ScienceDirect

ELSEVIER

Visualization of Functional Rotor Proteins of the Bacterial Flagellar Motor in the Cell Membrane

Hajime Fukuoka[1], Yoshiyuki Sowa[2], Seiji Kojima[1], Akihiko Ishijima[2] and Michio Homma[1]*

[1]*Division of Biological Science Graduate School of Biological Science, Nagoya University Chikusa-ku, Nagoya, 464-8602 Japan*

[2]*Department of Applied Physics Graduate School of Engineering Nagoya University Chikusa-Ku, Nagoya, 464-8603 Japan*

**Corresponding author*

The bacterial flagellar motor is a rotary motor driven by the electrochemical potentials of specific ions across the cell membrane. Direct interactions between the rotor protein FliG and the stator protein MotA are thought to generate the rotational torque. Here, we used total internal reflection fluorescent microscopy to observe the localization of green fluorescent protein (GFP)-fused FliG in *Escherichia coli* cells. We identified three types of fluorescent punctate signals: immobile dots, mobile dots that exhibited simple diffusion, and mobile dots that exhibited restricted diffusion. When GFP–FliG was expressed in a Δ*fliG* background, most of the cells were not mobile. When the cells were tethered to a glass side, however, rotating cells were commonly observed and a single fluorescent dot was always observed at the rotational center of the tethered cell. These fluorescent dots were likely positions at which functional GFP–FliG had been incorporated into a flagellar motor. Our results suggest that flagellar basal bodies diffuse in the cytoplasmic membrane until the axial structure and/or other structures assemble.

Keywords: bacterial flagella; FliG; stator; GFP

Introduction

Many bacteria sense external signals from the environment and can swim toward favorable conditions by rotating locomotive organelles called flagella. The bacterial flagellum consists of a helical filament that acts as a propeller, a basal body that acts as a rotary motor embedded in the cytoplasmic membrane, and a hook that acts as a universal joint connecting the filament to the basal body.[1] The rotary motor of a bacterial flagellum is driven by the flux of specific ions across the cell membrane; *Escherichia coli* and *Salmonella enterica* serovar *Typhimurium* use H^+, whereas marine *Vibrio* species and alkalophilic *Bacillus* species use Na^+.[2–4] In *Bacillus subtilis*, distinct stators for coupling either Na^+ or H^+ flux to force generation are thought to function in the same bacterial cell.[5]

The rotor in the flagellar basal body consists of an axial rod and two rings: the MS ring and the C ring. The MS ring is embedded in the cytoplasmic membrane, whereas the C ring is attached to the cytoplasmic surface of the MS ring. In Gram-negative bacteria, two additional rings, the L and P rings, surround the axial rod and are attached to the outer membrane and the peptidoglycan layer, respectively.[6] These rings are thought to act as bearings for the axial rod. During flagellar assembly, FliF first multimerizes to form the MS ring in the cytoplasmic membrane.[7] Next, FliG, FliM, and FliN assemble to form the C ring on the cytoplasmic surface of the MS ring.[6] The axial proteins are then exported to the outside of the cytoplasmic membrane by the export apparatus attached to the inside of the C ring to form the rod, hook, and flagellar filament.[8]

The stator of the flagellar motor consists of PomA and PomB in the Na^+-driven motors of *Vibrio alginolyticus*, or MotA and MotB in the H^+-driven motors of *E. coli*.[9–11] These stator complexes are

Present addresses: Y. Sowa, Clarendon Laboratory, University of Oxford, Parks Road, Oxford OX1 3PU, UK; A. Ishijima, Institute of Multidisciplinary Research for Advanced Materials, Tohoku University, Aoba-ku, Sendai, 980-8577, Japan.

Abbreviations used: GFP, green fluorescent protein; TIR, total internal reflection; CW, clockwise; CCW, counterclockwise.

E-mail address of the corresponding author: g44416a@cc.nagoya-u.ac.jp

thought to function as specific ion channels.[12,13] The A and B stator subunits are incorporated into the motor as a stator complex after completion of the hook-basal body; deletions in the C-terminal domain of the B subunit have been shown to block this incorporation process.[14,15] FliG, a cytoplasmic protein that is thought to be directly involved in force generation by the flagellar motor, forms the switch complex with FliM and FliN that changes the direction of motor rotation between clockwise (CW) and counterclockwise (CCW) in response to chemotactic signals.[16–19] Mutational analyses of the H^+-driven flagellar motor have identified charged residues in the C-terminal region of FliG and the cytoplasmic domain of MotA that are important for force generation.[20,21] In the crystal structure of the middle and C-terminal domains of *Thermotoga maritima* FliG, the corresponding charged residues are aligned in a C-terminal ridge that is exposed on the surface of the FliG molecule.[22] It has been predicted that the electrostatic interactions between the charged residues of FliG and the cytoplasmic regions of MotA cause motor rotation.[23] The precise mechanism underlying motor rotation, however, is not fully understood.

FliG molecules of the flagellar rotor have been visualized at the base of the polar flagellum in *V. alginolyticus* using fusion proteins carrying green fluorescent protein (GFP).[24] Moreover, FliG molecules tagged with yellow fluorescent protein were detected as several fluorescent foci on the surface of the cell body of *S. typhimurium*, a bacterium that has peritrichous flagella.[25] In the present work, we constructed functional fusion proteins of GFP and the *E. coli* rotor protein FliG and observed the rotating motor using total internal reflection (TIR) fluorescent microscopy.

Results

Motility of cells producing GFP–FliG

The *gfp* gene was genetically fused to the 5′ end of the *fliG* gene to form the *gfp-fliG* construct, the product of which was GFP–FliG. Wild-type *fliG* and *gfp-fliG* were cloned and placed under the control of arabinose-inducible promoters in the pYF2 and pYF1 plasmids, respectively. We investigated the motility of the cells producing GFP–FliG or wild-type FliG as a rotor component in semi-solid agar containing arabinose. In a medium containing 0.0005% (w/v) arabinose, Δ*fliG* cells (DFB225) producing wild-type FliG from pYF2 showed the same degree of swarming as RP437 cells, a strain with wild-type motility and chemotaxis (Figure 1(a)). Δ*fliG* cells producing wild-type FliG needed at least 0.0002% arabinose in the medium to achieve the same degree of motility as RP437 cells (data not shown), and the cells overproduced the FliG protein when they were placed in the medium containing 0.0002% arabinose (Figure 1(a)). On the other hand,

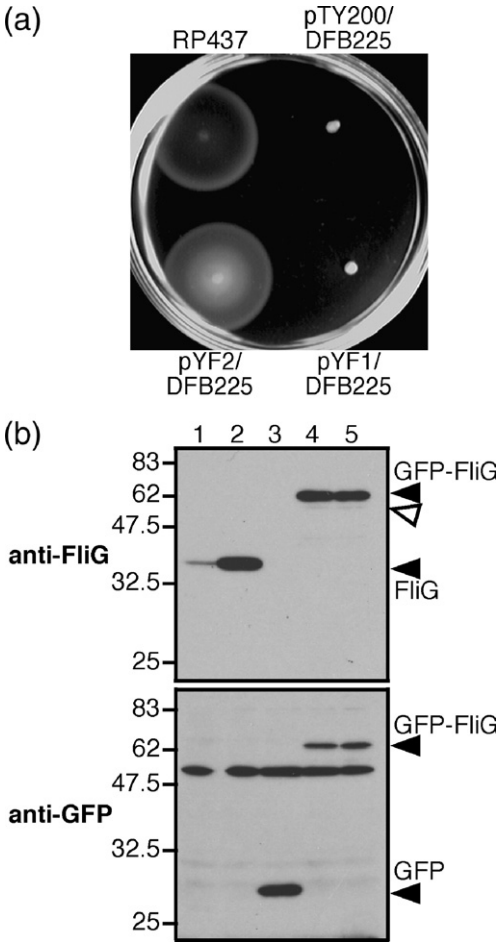

Figure 1. (a) Swarming behavior of cells producing GFP–FliG. pYF1 (encoding *gfp-fliG*)-carrying DFB225 cells, pYF2 (encoding wild-type *fliG*)-carrying DFB225, pTY200 (encoding *gfp*)-carrying DFB225 cells, and pBAD33 (vector)-carrying RP437 cells were grown in TG-0.27% (w/v) soft agar medium containing 0.0005% (w/v) arabinose at 30 °C for 9 h. RP437, wild-type for chemotaxis; DFB225, Δ*fliG* strain. (b) Immunoblots for GFP–FliG or wild-type FliG in whole-cell extracts. Proteins were detected with anti-FliG antibodies or anti-GFP antibodies. Molecular mass values (kDa) are shown on the left side of the panels. The band between 47.5 kDa and 62 kDa is probably a non-specific band detected by the anti-GFP antibodies because the band was detected in all of the lanes. Lane 1, pBAD33-carrying RP437 cells grown in TG medium containing no arabinose; lane 2, pYF2-carrying DFB225 cells grown in TG-0.0002% arabinose medium; lanes 3 and 4, pTY200-carrying and pYF1-carrying DFB225 cells grown in TG-0.0005% arabinose medium, respectively; lane 5, pYF1-carrying RP3098 cells (Δ*flhDC*) grown in TG-0.002% arabinose medium. Cells were grown at 30 °C for 4 h.

the Δ*fliG* cells producing GFP–FliG from pYF1 did not swarm in the semi-solid agar containing 0.0005% arabinose (Figure 1(a)). Under a light microscope, however, Δ*fliG* cells producing GFP–FliG were observed to swim, although their swimming ability was much lower than that of wild-type cells (Table 1). Similar amounts of plasmid-derived wild-type FliG and GFP–FliG proteins were detected by

Table 1. Motility parameters of the cells

Strains	FliG variants	Swimming fraction (%)[a]	Swimming speed (μm/s)[b]
DFB225	GFP–FliG	3±3	12±3
DFB225	Wild-type	85±6	26±4
RP437	Wild-type[c]	96±3	28±6

The cells were grown in media containing no arabinose (RP437), 0.0002% arabinose (DFB225 cells harboring the plasmid encoding *fliG*), or 0.0005% arabinose (DFB225 cells harboring the plasmid encoding *gfp-fliG*).

[a] The average value calculated from more than eight visual fields.

[b] The average value calculated from more than 40 cells.

[c] Wild-type FliG encoded on the chromosome.

immunoblot analysis of whole-cell extracts from the Δ*fliG* cells (Figure 1(b)). On the other hand, the cells producing GFP–FliG showed a reduced level of flagellin expression (Figure 2); the intensity of the band of flagellin derived from these cells was approximately ten times less than the intensity of the band derived from the cells producing wild-type FliG. In addition, the number and the length of the flagella observed with electron microscopy were greatly reduced in the cells producing GFP–FliG (data not shown). Thus, the fusion of the GFP molecule to FliG probably affected flagellar assembly.

Next, to investigate the function of individual motors, the cells were tethered to the surface of a coverslip using the FliC sticky filament, which has been shown to readily attach to glass surfaces.[26,27] FliC sticky proteins were produced from a second plasmid, pYS11.[27] The tethered cells robustly rotated on the coverslip in spite of their weak motility in liquid media. Immunoblot analysis of whole-cell extracts detected GFP–FliG at a position corresponding the expected molecular mass of 64 kDa (Figure 1). Very weak bands were detected just under the GFP–FliG bands (Figure 1(b), open arrowhead); these bands may have resulted from a slight degradation or mistranslation of GFP–FliG. Degradation products with a molecular mass corresponding to that of wild-type FliG, however, were not detected, indicating that GFP–FliG was functional in individual flagellar motors. The

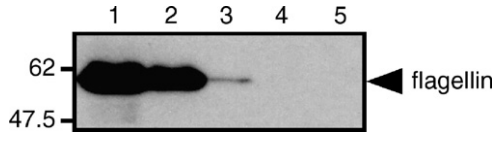

Figure 2. Detection of flagellin. Proteins were separated and immunoblotting was performed using anti-flagellin antibodies. Lane 1, pBAD33-carrying RP437 cells grown in TG medium containing no arabinose; lane 2, pYF2-carrying DFB225 cells grown in TG-0.0002% arabinose medium; lane 3, pYF1-carrying DFB225 cells grown in TG-0.0005% arabinose medium; lanes 4 and 5, pBAD33-carrying DFB225 cells and pTY200-carrying RP3098 cells grown in TG medium containing no arabinose, respectively.

rotational velocities of the tethered cells producing wild-type FliG and GFP–FliG were ca 6 and ca 3 revolutions/s, respectively (Table 2). For the wild-type FliG motor, the switching frequency and the percentage of time spent rotating CCW were 0.9 reversal/s and 65%, respectively. On the other hand, the switching frequency and the percentage of time the motor rotated CCW for the GFP–FliG motor were 0.4 reversal/s and more than 92%, respectively. Flagellar motors that incorporated GFP–FliG preferentially rotated CCW. Although the activity of the GFP–FliG motors was lower than that of the wild-type motors, the GFP-FliG motors were sufficiently functional for further analysis.

Subcellular localization of GFP–FliG

We observed the localization of GFP–FliG in the Δ*fliG* and Δ*flhDC* strains. Because the *flhDC* genes are master genes that control the expression of all of the flagellar genes, the Δ*flhDC* strain produces no flagellar components. Similar amounts of GFP–FliG protein were detected by immunoblot analysis of whole-cell extracts from the two cell lines (Figure 1(b), lanes 4 and 5). When cells at mid-log phase were immobilized on the surface of a polylysine-coated coverslip and observed using TIR fluorescent microscopy, we detected 5±1 (mean±SD) fluorescent dots near the cell surface in each of the Δ*fliG* cells producing GFP–FliG (Figure 3; Δ*fliG*, TIR). On the other hand, in the Δ*flhDC* cells producing GFP–FliG, no fluorescent dots were detected and a diffuse fluorescent signal was observed throughout the cell body (Figure 3; Δ*flhDC*, TIR). Using axial (brightfield) epi-illumination (epi-illumination), GFP–FliG was also detected throughout the cell bodies of the Δ*flhDC* cells (Figure 3; Δ*flhDC*, Epi). Therefore, the clustering of the GFP–FliG molecules was dependent on flagellar structures or one or more of the flagellar proteins. Under epi-illumination, we detected 11±3 fluorescent dots in each Δ*fliG* cell though the background fluorescent signal was larger than that observed using TIR illumination (Figure 3; Δ*fliG*, Epi and TIR). The number of fluorescent dots in each cell was more than the

Table 2. Rotational parameters of the cells

Strains	FliG variants	Rotational velocity[a]	Rotational bias[b]	Switching frequency[c]
DFB225	GFP-FliG	3±2	92±15	0.4±0.4
DFB225	Wild type	6±2	65±19	0.9±0.8

More than 40 tethered cells were investigated. Images were captured at 60 frames/s and 600 frames (10 s) were analyzed. The cells were grown in media containing 0.0002% arabinose (DFB225 cells harboring the plasmid encoding *fliG*), or 0.0005% arabinose (DFB225 cells harboring the plasmid encoding *gfp-fliG*).

[a] Rotation velocity is shown in revolutions/s.

[b] Rotational bias is shown as the percentage of time spent rotating CCW.

[c] Switching frequency is shown as the number of reversals/s.

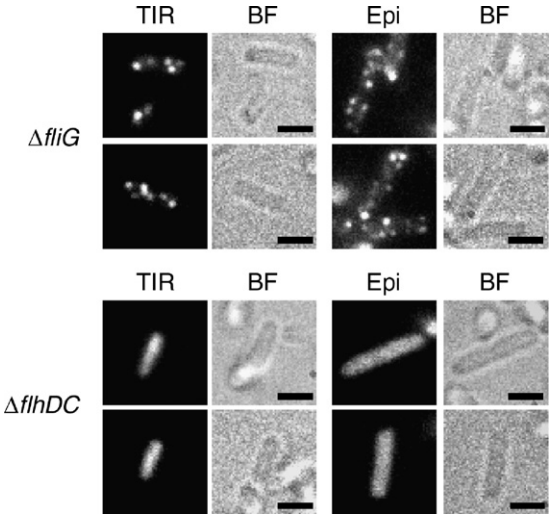

Figure 3. Sub-cellular localization of GFP–FliG. Cells producing GFP–FliG were grown at 30 °C for 4 h in medium containing 0.0005% arabinose (Δ*fliG*) or 0.002% arabinose (Δ*flhDC*), and were observed with a fluorescence microscope. TIR indicates the images obtained under TIR illumination, whereas Epi indicates images obtained under axial (brightfield) epi-illumination. BF indicates bright field images. The adjacent fluorescent and bright field images are images of the same cells. The bar represents 1.6 μm.

reported number of flagella for an *E. coli* cell.[28,30] This was probably due to flagellar basal bodies that lacked flagellar filaments.

Movement of GFP–FliG on the cytoplasmic membrane

In the Δ*fliG* cells producing GFP–FliG, we tracked the movement of the fluorescent dots in the cell membrane using TIR fluorescent microscopy. After the cells were immobilized on a polylysine-coated coverslip, we detected immobile and mobile fluorescent dots on the cell membrane (Figure 4). In each cell, approximately two immobile and four mobile fluorescent dots were detected. The positional distributions of the centers of the immobile dots on the cell membrane were restricted to a very narrow area (Figure 4(d)). On the other hand, as shown in Figure 4(a) and (b), one fluorescent dot (dot 1) moved in the direction of the cell pole, whereas the movement of another fluorescent dot (dot 2) was restricted within a limited region for more than 12 s. We analyzed the movement of these mobile dots by plotting the mean squared displacement *versus* the time interval (*MSD*-Δ*t*) and examining the relative deviation. The *MSD*-Δ*t* plot for dot 1 appeared to fit a linear function, which is indicative particle undergoing simple diffusion (Figure 4(c)). On the other hand,

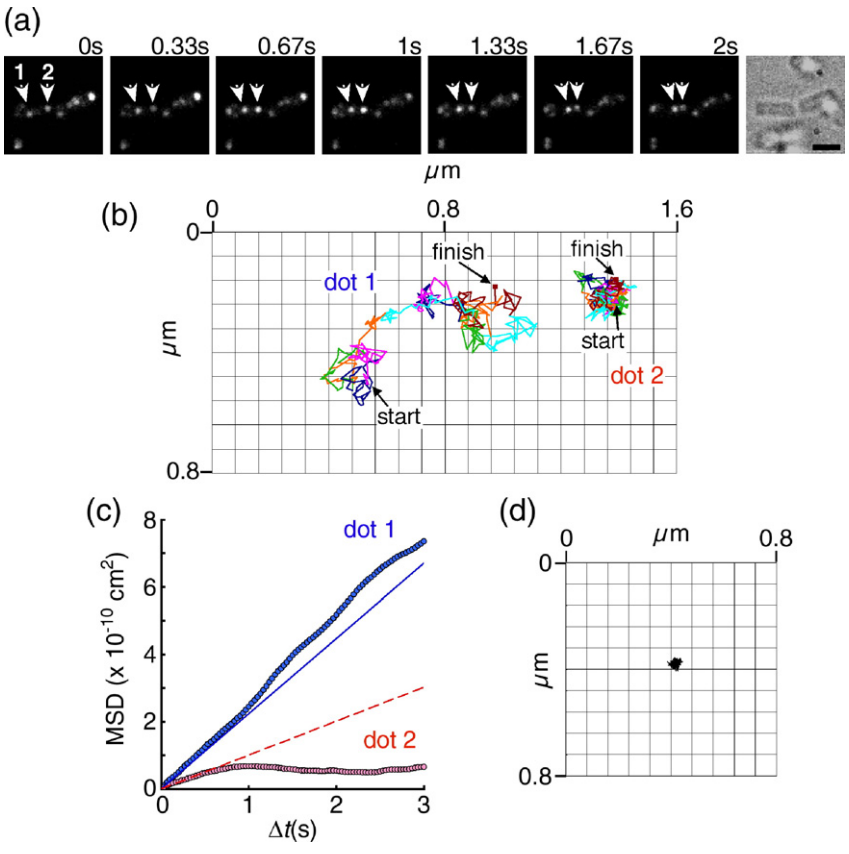

Figure 4. Movement of the fluorescent dots. (a) A sequence of images (TIR illumination) of fluorescent dots formed by GFP–FliG. The Figure shows a 2 s image sequence, and every tenth frame is shown. Images were captured at a normal video rate (30 frames/s). The bar represents 1.6 μm. (b) Movement trajectories of fluorescent dot 1 and fluorescent dot 2 (arrowheads 1 and 2 in (a), respectively). Trajectories of the centers of the fluorescent dots over 12 s are shown. Each trajectory color represents the movement of the dot during a period of 1 s, and the movements of the dots in first second through the sixth second are denoted in pink, blue, green, orange, turquoise, and red, respectively; this order of the colors is then repeated for the movements of the dots in the seventh second through the 12th second. Start and finish indicate the position of the dot in the first video frame and the last video frame, respectively. (c) *MSD*-Δ*t* plots for the trajectories of the fluorescent dots. Blue and red circles indicate the *MSD*-Δ*t* plots for dot 1 and dot 2, respectively. The blue continuous line and the red broken line are the linear-fitted lines at 2Δ*t*, 3Δ*t*, and 4Δ*t* for the *MSD* values (Δ*t* is the video frame time: 33 ms). *RD* (*N*, *n*) was calculated as described in Materials and Methods. (d) Trajectory of an immobile fluorescent dot in another cell.

the *MSD*-Δ*t* plot of dot 2 is characteristic of a particle undergoing restricted diffusion (Figure 4(c)). The relative deviation, *RD* (300, 90), of dot 1 and dot 2 were calculated to be 1.1 and 0.2, respectively. From a comparison with the theoretical *RD* (300, 90) reported by Kusumi *et al.*,[29] the trajectory of dot 1 was determined to be a result of simple diffusion, whereas the trajectory of dot 2 was determined to be a result of restricted diffusion. We analyzed the trajectories of 15 other fluorescent dots using *RD* (300, 90) or *RD* (200, 90). Three of these trajectories were determined to result from simple diffusion and the average *RD* value for these dots was 0.9. Eight of the trajectories were determined to result from restricted diffusion and the average *RD* value for these dots was 0.2. The diffusion modes of the four remaining dots were not determined, because there were not enough data points for analysis. Estimating the diffusion coefficients (*D*) of dot 1 and dot 2 using the slope of each of the *MSD*-Δ*t* plots revealed that the diffusion coefficients of dot 1 and dot 2 were 5.6×10^{-11} cm^2/s and 2.5×10^{-11} cm^2/s, respectively. The average diffusion coefficient for all 17 of the mobile dots was 4.9×10^{-11} ($\pm3.1\times10^{-11}$)cm^2/s.

Observation of GFP–FliG in tethered cells

If the GFP–FliG protein retains its function and attaches to basal bodies as a component of the rotor, the rotational center of each tethered cell should be fluorescently labeled (Figure 5(a), central dot). To determine the position of the rotational center, we chose slowly rotating cells (approximately 1 revolution/s). For each of the GFP–FliG-producing cells, a single immobile fluorescent dot was observed at the midpoint of the cell body, which was the rotational center of the tethered cell (Figure 5(b), arrowhead C). In order to precisely determine the position of the central dot and the rotational center of the tethered cell, we determined the centers of the fluorescent signals from a central dot (arrowhead C)

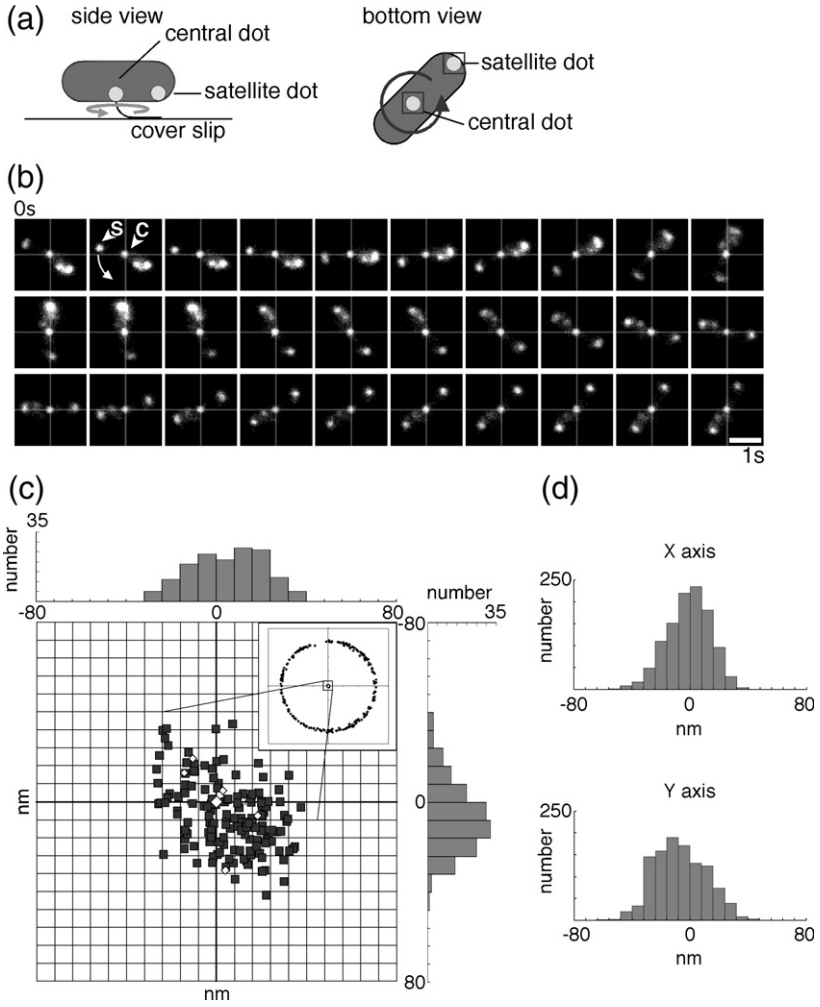

Figure 5. Sub-cellular localization of GFP–FliG in a tethered cell and determination of the rotational center. (a) Schematic diagrams to illustrate the concept. A flagellar filament (sticky filament) extending from the cell body is immobilized on the coverslip and the cell body rotates around this point. Central and satellite fluorescent dots are localized at the rotational center and the cell pole, respectively. These two dots were used to define the rotational center of the tethered cell. (b) A sequence of fluorescent images of a tethered cell. Images were captured at the normal video rate (30 frames/s) and every frame in the sequence is shown. C denotes the central dot and S marks the satellite dot. The bar represents 1.6 μm. (c) The distributions of the positions of a satellite dot and a central dot in a tethered cell. Shaded squares indicate the distribution of the positions of the central dot (150 points). The small open squares indicate the centers of the ellipses fitted from each rotation of the satellite dot (we analyzed five rotations). The positions of the centers of the fitted ellipses were calculated using the least-squares method from the center of the satellite dot. In this Figure, the position of the rotational center (large open square) was defined as the average position of the five small open squares. The origin of this graph represents the center of the ellipse fitted based on the rotation of the satellite dot. Histograms indicate the distributions of the central dot along the *X* axis and *Y* axis. (d) Histograms of positional data obtained for central dots from 11 tethered cells. For each tethered cell, the positions of the central dot were obtained from 100 frames, and the range of the distribution of the central dots was normalized to the center of the fitted ellipse.

and a satellite dot (arrowhead S) (Figure 5(a) and (b)) from more than 100 frames (images were captured at 30 frames/s). As shown in the inset in Figure 5(c), the center of the satellite dot followed a circular path with a radius of approximately 1.2 μm (shaded squares). The rotational center of the tethered cell was defined as the center of the ellipse calculated by least-squares fitting of the trajectory of the center of the satellite dot (Figure 5(c), large open square). In this cell, the standard deviations for the center of the fitted ellipse were ±12.8 nm along the *X* axis and ±19.2 nm along the *Y* axis. The positions of the center of the central dot were distributed within a range of approximately 80 nm along both the *X* and *Y* axes (Figure 5(c), shaded squares). The rotational center calculated from the path of the satellite dot was located within the area defined by the distribution of the positions of the central dot (Figure 5(c)). Figure 5(d) shows the distributions of the positions of the central dots from 11 tethered cells. For each of these cells, the rotational center calculated from the movement of a satellite dot was located within the range defined by the distribution of the positions of the central dot. These results indicate that the GFP–FliG molecules localized at the rotational centers of the tethered cells.

Discussion

The bacterial flagellar motor is a rotary motor driven by the electrochemical potentials of ions. The interaction between the rotor and the stators is thought to generate torque, thereby converting the energy of ion flux into mechanical power. In the flagellar motor of *E. coli*, FliG is a rotor component that is thought to interact directly with the stator complex formed by MotA and MotB.[23] Here, we used the functional fusion protein GFP–FliG and TIR fluorescent microscopy to observe rotating motors and to characterize the motion of basal bodies in the cell membrane of *E. coli*.

To construct a flagellum, FliF first assembles to form the MS ring in the cytoplasmic membrane. FliG then attaches to the cytoplasmic surface of the MS ring to form the C ring with FliM and FliN.[6,7] In the Δ*flhDC* deletion strain, the MS ring is not formed because none of the flagellar proteins, including FliF, are produced.[1] Accordingly, no fluorescent dots were observed in GFP–FliG-producing Δ*flhDC* cells; a diffuse fluorescent signal was instead detected throughout the Δ*flhDC* cells (Figure 3). In contrast, fluorescent dots were detected in GFP–FliG-producing Δ*fliG* cells, indicating that the formation of the fluorescent dots was dependent on the flagellar proteins. It can be concluded that the fluorescent dots corresponded to locations at which GFP–FliG bound to MS rings, and in some cases, assembled to form the rotor in the basal body of a flagellar motor.

Although we may not have detected all of the fluorescent dots due to the high background fluorescence, at least 11 fluorescent dots were observed in each cell. Interestingly, this number of dots is more than the reported number of flagella for an individual cell.[28,30] The larger than expected number of fluorescent puncta was probably not due to the overproduction of GFP–FliG. In Δ*fliG* cells, the number of MS rings is probably the same as in RP437 cells because FliF is produced from the chromosome. This means that the number of fluorescent dots was limited by the number of MS rings. Thus, the maximum number of fluorescent dots would not exceed the number of MS rings even if GFP–FliG was overproduced. Therefore, *E. coli* cells must have complete flagellar structures and partial flagella that lack filaments, such as basal bodies that are not completely assembled and/or basal bodies that have lost the flagellar filaments. It has been reported that there are an average of 3.4 flagella in each *E. coli* cell.[30] This suggests that there are twice as many unfinished basal body structures as there are fully assembled basal bodies with intact flagella.

We observed mobile and immobile fluorescent dots in cells producing GFP–FliG. After the construction of the MS ring and the C ring, the export apparatus attached to the inside of the C ring transports the axial proteins outside of the cytoplasmic membrane, where they assemble to form the rod, hook, and filament.[8] Structures consisting of an MS ring and a C ring without the axial components can probably diffuse in the cell membrane, whereas basal bodies with axial structures that penetrate the peptidoglycan layer and/or the outer membrane are likely fixed in the cell membrane. The diffusion coefficient of the mobile fluorescent dots roughly estimated from the *MSD*-Δ*t* plots was $4.9\times10^{-11}(\pm3.1\times10^{-11})$ cm^2/s. If each mobile fluorescent dot corresponded to a single flagellar basal body, the molecular size of the fluorescent dots was at least 3200 kDa (26 molecules each of FliF, FliG, and GFP). In the cell membrane of *E. coli*, the diffusion coefficient (*D*) of a TatA–GFP fusion protein (9.6 kDa) was estimated to be 1.3×10^{-9} cm^2/s using fluorescence recovery after photobleaching.[31] On the other hand, the *D* value of the $MotA_4$–$MotB_2$ complex, which is the stator of the bacterial flagellar motor, was estimated to be 8.8×10^{-11} cm^2/s using single particle tracking.[32] Because the *D* value is dependent on the Stokes radius (*r*) of the transmembrane domain in the lipid bilayer, it is not surprising that the *D* values of the complexes composed of GFP–FliG and $MotA_4$–$MotB_2$ are of the same order of magnitude ($\times10^{-11}$ cm^2/s). On the other hand, the observation that the *D* value of the GFP–FliG complex is smaller than that reported for the TatA fusion protein is reasonable, because TatA was predicted to have one transmembrane segment by the SOSUI program.

Some of the mobile fluorescent dots diffused within a restricted area (Figure 4(b) and (c), dot 2). Structures in the peptidoglycan layer and/or the outer membrane, such as L rings and P rings, might capture flagellar basal bodies that are diffusing in the cytoplasmic membrane. On the other hand, in eukaryotic cells, several elements have been

proposed to restrict the movement of membrane proteins, including a membrane skeleton/cytoskeleton fence or transient confinement zones (TCZs).[33–35] In bacteria, MreB forms actin-like filaments that run along the inner surface of the cytoplasmic membrane,[36] whereas FtsZ, a tubulin homolog that is required for cell division, forms a ring structure at the site of division.[37] Membrane domains enclosed by cytoskeletal-like structures or TCZ-like membrane domains might restrict the diffusion of flagellar basal bodies. This restriction might be involved in determining positions at which flagella form.

Only 3% of cells producing GFP–FliG were observed to swim, and the swimming speed of these cells was half of the speed observed for cells producing wild-type FliG from a plasmid. This phenotype may be attributable to a reduction in the number of flagella. The percentage of GFP–FliG-producing cells with flagella was low and the amount of flagellin in these cells was approximately ten times less than the amount of flagellin in the cells producing wild-type FliG. The *fliC* gene, which encodes flagellin, is a class III gene in the expression hierarchy of the flagellar genes. The expression of class III genes is repressed by the anti-sigma factor FlgM, and this repression is removed following the excretion of FlgM through the flagellar export apparatus.[1] The low expression level of flagellin suggests that anti-sigma factor FlgM was not efficiently pumped out of the GFP–FliG-producing cells; this would prevent the cells from down-regulating the expression of the class II flagellar genes and increasing the expression of the class III genes. Our observations suggest that the activity of the export apparatus was reduced or the assembly of the export apparatus was inhibited by the GFP molecule fused to FliG.

When the GFP–FliG-producing cells were tethered to glass coverslips, they were able to rotate although the rotation speed was about half of that observed for cells producing wild-type FliG. A puncta of GFP–FliG was localized at the rotational center of each tethered cell (Figure 5). This indicates that (i) GFP–FliG was located at the site of the motor, (ii) GFP–FliG assembled on an MS ring or in a flagellar basal body, and (iii) the fusion protein functioned as a component of the rotor in the flagellar motor. Compared to cells with wild-type motors, the rotation of the motors was biased to the CCW direction and the switching frequency was low in the GFP–FliG-expressing cells. GFP is a large protein (27 kDa) with a β-barrel structure.[38] Fusion of this protein to the N terminus of FliG may have affected the structure of FliG, the interaction between FliG and MotA, and/or the interaction between FliM and phosphorylated CheY, which switches the rotation of the motor from CCW to CW. Alternatively, the low level of expression of the class III genes or the late genes (the *che* and *mot* genes) might have affected the rotation of the motor.[1]

Here, we have successfully observed fluorescently labeled, rotating flagellar motors and the diffusion of flagellar basal bodies in the cytoplasmic membrane. We do not know the precise number of FliG molecules that are in an individual rotating motor. According to a rough estimate, the fluorescent intensity of one of the fluorescent dots appeared to be about ten times stronger than that of a single molecule of GFP (data not shown), suggesting that at least ten molecules of GFP–FliG were present in each fluorescent dot. As shown in a recent report,[32] we may be able to determine the precise number of FliG molecules that are incorporated into a functional motor by measuring single-step photobleaching of GFP–FliG in a rotating cell. Additionally, development of this technique may allow us to examine the interaction between the flagellar motor components, such as the rotor and the stator, using fluorescence resonance energy transfer.

Materials and Methods

Bacterial strains, growth conditions, and media

The bacterial strains used in this study are listed in Table 3. *E. coli* cells were cultured in LB broth (1% (w/v) tryptone peptone, 0.5% (w/v) yeast extract, and 0.5% (w/v) NaCl) or TG broth (1% (w/v) tryptone peptone, 0.5% (w/v) NaCl, and 0.5% (w/v) glycerol) at 30 °C. Chloramphenicol was added to a final concentration of 25 μg/ml and ampicillin was added to a final concentration of 50 μg/ml.

Plasmids

The plasmids used in this study are listed in Table 3. The plasmids carrying the *fliG* gene under the control of the *araBAD* promoter were pBAD33-based plasmids. The SacI/HindIII fragment from pSL27 was inserted into the SacI/HindIII sites of pTY102, resulting in the pYF2 plasmid. A fragment encoding the *fliG* gene, which was amplified by PCR using pYF2 as a template, the sense primer BsrGI–*fliG*, and an antisense primer that annealed to a region downstream of the multiple cloning site was

Table 3. Bacterial strains and plasmids

	Description	Source or reference
A. *Strains*		
RP437	F⁻ *thi thr leu his met eda rpsL* (wild-type for motility)	41
DFB225	RP437 Δ*fliG*	42
RP3098	Δ(*flhD–flhA*)*4*	43
B. *Plasmids*		
pBAD33	Cm^r, P*BAD*	44
pBR322	Ap^r, Tc^r	45
pTY200	*his6-gfp* in pBAD33	24
pTY102	*fliG* of *V. alginolyticus* in pBAD33	24
pSL27	*fliG* of *E. coli* in pAlter-1	41
pYF2	*fliG* of *E. coli* in pBAD33	This work
pYF1	*his6-gfp-fliG* of *E. coli* in pBAD33	This work
pYS11	*fliC sticky* in pBR322	27

Cm^r, chloramphenicol resistant; Ap^r, ampicillin resistant; Tc^r, tetracycline resistant; P*BAD*, *araBAD* promoter; his6, hexahistidine tag.

inserted into the BsrGI/HindIII sites of pTY200; this plasmid was named pYF1.

Preparation of cells for observation with fluorescence microscopy

Overnight cultures of cells harboring the plasmids were inoculated into TG medium (1/100) in the presence of arabinose and cultured at 30 °C for 4 h. The cells were harvested by centrifugation and suspended in motility medium: 10 mM potassium phosphate (pH 7.0), 0.1 mM EDTA, and 85 mM NaCl. Sixty μl of the cell suspension was loaded into the space between a slide glass and a coverslip with a spacer. The slide was then inverted and incubated for 2 min. Another 60 μl of motility medium was loaded into the space between the slide and the coverslip to remove the remaining unattached cells.

Microscopic system

We used an Olympus IX-71 microscope with a modified mirror turret to allow side entry of the excitation light into the microscope. A laser beam ($\lambda = 488$ nm) for excitation was focused at the back focal plane of the objective lens (Olympus PLAPON 60XOTIRFM, NA = 1.45). For objective TIR illumination[39] the angle of the incident laser beam was adjusted with a mirror set in front of the focusing lens ($f = 180$) so that the laser beam would pass near the edge of the objective lens. In our experiments, the incidence angle was 71.4°, and thus the evanescent light reached a depth of approximately 70 nm (the value when the sample on the glass surface was water). The image was projected to an EM-CCD camera (DV860-BV, Andor Technology, South Windsor, CT) through a projection lens (5×); as a result, 1 pixel corresponded to 80 nm in the specimen plane. All images were captured at the normal video rate (30 frames/s). We confirmed the positional resolution of this microscope system was 5 nm in an experiment using a 100 nm fluorescent bead.

Determination of the rotational center of a tethered cell

We used the free ImageJ software† for analysis of all of the images. The position of the rotational center was defined as the center of a fitted ellipse calculated by the least-squares method from the center of a fluorescent satellite dot. For the definition of the rotational center of a tethered cell, the positions of the center of the fluorescent satellite dot obtained from more than 100 video frames were used. The distribution of positions of the central dots was calculated from the centers of their fluorescent signals. To calculate the center of each dot, we analyzed video frames that contained more than 16 pixels that were brighter than the threshold intensity. We selected tethered cells rotating CCW for analysis.

Tracking the movement of fluorescent dots

To track the movement of the mobile fluorescent dots, Δ*fliG* cells producing GFP–FliG were attached to poly-lysine-coatedcoverslips and observed with TIR fluorescent microscopy. Images were captured at 30 frames/s and the center of the fluorescent mobile dot was calculated in each video frame. For the trajectory of each fluorescent dot, the mean square displacement (*MSD*) was calculated according to the following formula:[29]

$$MSD(n\delta t) = \frac{1}{N-1-n}\sum_{j=1}^{N-1-n}\left\{\left[x(j\delta t + n\delta t) - x(j\delta t)\right]^2 + \left[y(j\delta t + n\delta t) - y(j\delta t)\right]^2\right\},$$

where δt is the video frame time (33 ms) and $(x(j\delta t + n\delta t) - x(j\delta t), y(j\delta t + n\delta t) - y(j\delta t))$ describes the position of the dot following a time interval $\Delta t_n = n\delta t$ after starting at position $(x(j\delta t), y(j\delta t))$; N is the total number of frames in the recording sequence, n and j are positive integers, and n determines the time increment. The diffusion coefficients (D_{2-4}) of the mobile dots were estimated by fitting the *MSD* values at $2\Delta t$, $3\Delta t$, and $4\Delta t$ using a straight line.[29] Mobile dots that were tracked for more than 200 frames were analyzed for the calculation of the diffusion coefficient. The relative deviation $RD(N, n)$ was used for the determination of the diffusion mode of a mobile fluorescent dot.[29] The relative deviation is defined as

$$RD(N, n) = \frac{MSD(N, n)}{4D_{2-4n\delta t}}$$

where $MSD(N, n)$ represents the *MSD* at the time interval $n\delta t$ from a sequence of N video frames. $4D_{2-4}$ is the expected average *MSD* value for fluorescent dots undergoing simple diffusion with a diffusion coefficient of D_{2-4}. The value of RD (300, 90) or RD (200, 90) was used for the determination of the diffusion mode of each mobile fluorescent dot.[29]

Detection of GFP–FliG and flagellin in *E. coli* cells

E. coli cells harboring a plasmid encoding wild-type FliG or GFP–FliG were incubated at 30 °C for 4 h in TG medium containing arabinose. The cells were harvested by centrifugation and suspended in motility medium to an A_{660} of 10. The same volume of SDS loading buffer (033M Tris-HCl, pH 6.8, 42% glycerol, 5% SDS, 0.017% bromophenol blue, 17% 2-mercaptoethanol) was added to the cell suspensions and the samples were boiled at 100 °C for 5 min. The proteins were separated by SDS–PAGE and immunoblotting was performed using anti-FliG (a gift from D. Blair) and anti-GFP antibodies (GFP monoclonal antibodies, Clontech).

To detect flagellin, a 1/10 volume of trichloroacetic acid was added to the cell culture ($A_{660} = 1$) and the cells were harvested by centrifugation. The pellet was washed with acetone and dried. The pellet was suspended in a 1/10 volume of the twofold diluted SDS loading buffer to the original culture volume. The proteins were separated by SDS–PAGE and immunoblotting was performed using anti-flagellin antibodies (laboratory stock).

Measurement of the swimming fraction and swimming speed

Cells were grown at 30 °C for 4 h in TG medium containing arabinose. The cell suspensions were diluted 50-fold in fresh TG medium containing 20 mM serine, which was used to suppress CW rotation. Cell motility was observed under a dark-field microscope and recorded on videotape. Swimming speed was determined as

† http://rsb.info.nih.gov/ij/

described.[40] The average swimming speed was obtained by measuring at least 40 swimming tracks. The swimming fraction was measured from the same videotape.

Acknowledgements

We are grateful to Dr Richard Berry for critically reading the manuscript and thank Dr Toshiharu Yakushi for helpful discussions. This work was supported in part by grants-in-aid for scientific research from the Japan Society for the Promotion of Science (to M. H. and S. K.), from the Ministry of Education, Culture, Sports, Science and Technology of Japan (to A. I.), from JSPS Research Fellowships for Young Scientists (to Y. S.), and from the Japan Science and Technology Agency (to M. H., S. K. and A. I.).

References

1. Macnab, R. M. (1996). Flagela and motility. In *Eschericia coli and Salmonella* (Neidhardt, F. C., ed), pp. 123–145, American Society for Microbiology, Washington, DC.
2. Atsumi, T., McCarter, L. L. & Imae, Y. (1992). Polar and lateral flagellar motors of marine *Vibrio* are driven by different ion-motive forces. *Nature*, **355**, 182–184.
3. Hirota, N., Kitada, M. & Imae, Y. (1981). Flagellar motors of alkalophilic *Bacillus* are powered by an electrochemical potential gradient of Na^+. *FEBS Letters*, **132**, 278–280.
4. Manson, M. D., Tedesco, P., Berg, H. C., Harold, F. M. & van der Drift, C. (1977). A proton motive force drives bacterial flagella. *Proc. Natl Acad. Sci. USA*, **74**, 3060–3064.
5. Ito, M., Hicks, D. B., Henkin, T. M., Guffanti, A. A., Powers, B. D., Zvi, L. *et al.* (2004). MotPS is the stator-force generator for motility of alkaliphilic *Bacillus*, and its homologue is a second functional Mot in *Bacillus subtilis*. *Mol. Microbiol.* **53**, 1035–1049.
6. Francis, N. R., Sosinsky, G. E., Thomas, D. & Derosier, D. J. (1994). Isolation, characterization and structure of bacterial flagellar motors containing the switch complex. *J. Mol. Biol.* **235**, 1261–1270.
7. Kubori, T., Shimamoto, N., Yamaguchi, S., Namba, K. & Aizawa, S. (1992). Morphological pathway of flagellar assembly in *Salmonella typhimurium*. *J. Mol. Biol.* **226**, 433–446.
8. Macnab, R. M. (2004). Type III flagellar protein export and flagellar assembly. *Biochim. Biophys. Acta*, **1694**, 207–217.
9. Asai, Y., Kojima, S., Kato, H., Nishioka, N., Kawagishi, I. & Homma, M. (1997). Putative channel components for the fast-rotating sodium-driven flagellar motor of a marine bacterium. *J. Bacteriol.* **179**, 5104–5110.
10. Dean, G. D., Macnab, R. M., Stader, J., Matsumura, P. & Burks, C. (1984). Gene sequence and predicted amino acid sequence of the motA protein, a membrane-associated protein required for flagellar rotation in *Escherichia coli*. *J. Bacteriol.* **159**, 991–999.
11. Stader, J., Matsumura, P., Vacante, D., Dean, G. E. & Macnab, R. M. (1986). Nucleotide sequence of the *Escherichia coli* MotB gene and site-limited inccorporation of its product into the cytoplasmic membrane. *J. Bacteriol.* **166**, 244–252.
12. Blair, D. F. & Berg, H. C. (1990). The MotA protein of *E. coli* is a proton-conducting component of the flagellar motor. *Cell*, **60**, 439–449.
13. Sato, K. & Homma, M. (2000). Functional reconstitution of the Na^+-driven polar flagellar motor component of *Vibrio alginolyticus*. *J. Biol. Chem.* **275**, 5718–5722.
14. Fukuoka, H., Yakushi, T., Kusumoto, A. & Homma, M. (2005). Assembly of motor proteins, PomA and PomB, in the Na^+-driven stator of the flagellar motor. *J. Mol. Biol.* **351**, 707–717.
15. Yakushi, T., Hattori, N. & Homma, M. (2005). Deletion analysis of the carboxyl-terminal region of the PomB component of the *Vibrio alginolyticus* polar flagellar motor. *J. Bacteriol.* **187**, 778–784.
16. Bren, A. & Eisenbach, M. (1998). The N terminus of the flagellar switch protein, FliM, is the binding domain for the chemotactic response regulator. *CheY. J. Mol. Biol.* **278**, 507–514.
17. Mathews, M. A., Tang, H. L. & Blair, D. F. (1998). Domain analysis of the FliM protein of *Escherichia coli*. *J. Bacteriol.* **180**, 5580–5590.
18. Toker, A. S. & Macnab, R. M. (1997). Distinct regions of bacterial flagellar switch protein FliM interact with FliG. *FliN and CheY. J. Mol. Biol.* **273**, 623–634.
19. Yamaguchi, S., Aizawa, S., Kihara, M., Isomura, M., Jones, C. J. & Macnab, R. M. (1986). Genetic evidence for a switchig and energy-transducing complex in the flagellar motor of *Salmonella typhimurium*. *J. Bacteriol.* **168**, 1172–1179.
20. Lloyd, S. A. & Blair, D. F. (1997). Charged residues of the rotor protein FliG essential for torque generation in the flagellar motor of *Escherichia coli*. *J. Mol. Biol.* **266**, 733–744.
21. Zhou, J. D. & Blair, D. F. (1997). Residues of the cytoplasmic domain of MotA essential for torque generation in the bacterial flagellar motor. *J. Mol. Biol.* **273**, 428–439.
22. Brown, P. N., Hill, C. P. & Blair, D. F. (2002). Crystal structure of the middle and C-terminal domains of the flagellar rotor protein FliG. *EMBO J.* **21**, 3225–3234.
23. Zhou, J. D., Lloyd, S. A. & Blair, D. F. (1998). Electrostatic interactions between rotor and stator in the bacterial flagellar motor. *Proc. Natl Acad. Sci. USA*, **95**, 6436–6441.
24. Yorimitsu, T., Mimaki, A., Yakushi, T. & Homma, M. (2003). The conserved charged residues of the C-terminal region of FliG, a rotor component of the Na^+-driven flagellar motor. *J. Mol. Biol.* **334**, 567–583.
25. Hirano, T., Shibata, S., Ohnishi, K., Tani, T. & Aizawa, S. (2005). N-terminal signal region of FliK is dispensable for length control of the flagellar hook. *Mol. Microbiol.* **56**, 346–360.
26. Ryu, W. S., Berry, R. M. & Berg, H. C. (2000). Torque-generating units of the flagellar motor of *Escherichia coli* have a high duty ratio. *Nature*, **403**, 444–447.
27. Sowa, Y., Rowe, A. D., Leake, M. C., Yakushi, T., Homma, M., Ishijima, A. & Berry, R. M. (2005). Direct observation of steps in rotation of the bacterial flagellar motor. *Nature*, **437**, 916–919.
28. Silverman, M. & Simon, M. I. (1974). Flagellar rotation and the mechanism of bacterial motility. *Nature*, **249**, 73–74.
29. Kusumi, A., Sako, Y. & Yamamoto, M. (1993). Confined lateral diffusion of membrane receptors as studied by single particle tracking (nanovid microscopy). Effects of calcium-induced differentiation in cultured epithelial cells. *Biophys. J.* **65**, 2021–2040.

30. Turner, L., Ryu, W. S. & Berg, H. C. (2000). Real-time imaging of fluorescent flagellar filaments. *J. Bacteriol.* **182**, 2793–2801.
31. Mullineaux, C. W., Nenninger, A., Ray, N. & Robinson, C. (2006). Diffusion of green fluorescent protein in three cell environments in *Escherichia coli*. *J. Bacteriol.* **188**, 3442–3448.
32. Leake, M. C., Chandler, J. H., Wadhams, G. H., Bai, F., Berry, R. M. & Armitage, J. P. (2006). Stoichiometry and turnover in single, functioning membrane protein complexes. *Nature*, **443**, 355–358.
33. Sako, Y. & Kusumi, A. (1994). Compartmentalized structure of the plasma membrane for receptor movements as revealed by a nanometer-level motion analysis. *J. Cell Biol.* **125**, 1251–1264.
34. Sheets, E. D., Lee, G. M., Simson, R. & Jacobson, K. A. (1997). Transient confinement of a glycosylphosphatidylinositol-anchored protein in the plasma membrane. *Biochemistry*, **36**, 12449–12458.
35. Simson, R., Yang, B., Moore, S. E., Doherty, P., Walsh, F. S. & Jacobson, K. A. (1998). Structural mosaicism on the submicron scale in the plasma membrane. *Biophys. J.* **74**, 297–308.
36. Shih, Y. L., Le, T. & Rothfield, L. (2003). Division site selection in *Escherichia coli* involves dynamic redistribution of Min proteins within coiled structures that extend between the two cell poles. *Proc. Natl Acad. Sci. USA*, **100**, 7865–7870.
37. Ben-Yehuda, S. & Losick, R. (2002). Asymmetric cell division in *B. subtilis* involves a spiral-like intermediate of the cytokinetic protein FtsZ. *Cell*, **109**, 257–266.
38. Yang, F., Moss, L. G. & Phillips, G. N., Jr (1996). The molecular structure of green fluorescent protein. *Nature Biotechnol.* **14**, 1246–1251.
39. Tokunaga, M., Kitamura, K., Saito, K., Iwane, A. H. & Yanagida, T. (1997). Single molecule imaging of fluorophores and enzymatic reactions achieved by objective-type total internal reflection fluorescence microscopy. *Biochem. Biophys. Res. Commun.* **235**, 47–53.
40. Atsumi, T., Maekawa, Y., Yamada, T., Kawagishi, I., Imae, Y. & Homma, M. (1996). Effect of viscosity on swimming by the lateral and polar flagella of *Vibrio alginolyticus*. *J. Bacteriol.* **178**, 5024–5026.
41. Parkinson, J. S. & Houts, S. E. (1982). Isolation and behavior of *Escherichia coli* deletion mutants lacking chemotaxis functions. *J. Bacteriol.* **151**, 106–113.
42. Lloyd, S. A., Tang, H., Wang, X., Billings, S. & Blair, D. F. (1996). Torque generation in the flagellar motor of *Escherichia coli*: evidence of a direct role for FliG but not for FliM or FliN. *J. Bacteriol.* **178**, 223–231.
43. Slocum, M. K. & Parkinson, J. S. (1983). Genetics of methyl-accepting chemotaxis proteins in *Escherichia coli*: organization of the tar region. *J. Bacteriol.* **155**, 565–577.
44. Guzman, L. M., Belin, D., Carson, M. J. & Beckwith, J. (1995). Tight regulation, modulation, and high-level expression by vectors containing the arabinose pBAD promoter. *J. Bacteriol.* **177**, 4121–4130.
45. Sutcliffe, J. G. (1978). Nucleotide sequence of the ampicillin resistance gene of *Escherichia coli* plasmid pBR322. *Proc. Natl Acad. Sci. USA*, **75**, 3737–3741.

Edited by J. Karn

(Received 24 August 2006; received in revised form 29 December 2006; accepted 4 January 2007)
Available online 12 January 2007